Atomic Force Microscopy Nanomanipulation of Shape Persistent, Spherical, Self-Assembled Aggregates of Gold Nanoparticles

Jeroen van Herrikhuyzen,[†] Ron Willems,[†] Subi J. George,[†] Cees Flipse,[†] Jeroen C. Gielen,[‡] Peter C. M. Christianen,[‡] Albertus P. H. J. Schenning,[†,*] and Stefan C. J. Meskers[†,*]

[†]Laboratory for Macromolecular and Organic Chemistry, Eindhoven University of Technology, PO Box 513, 5600MB Eindhoven, The Netherlands, and [‡]High Field Magnet Laboratory, Institute for Molecules and Materials, Radboud University Nijmegen, Toernooiveld 7, 6525 ED Nijmegen, The Netherlands

ABSTRACT Gold (Au) nanoparticles have been synthesized that are stabilized by an organic ligand bearing a dithiolane functional group for binding to Au, an oligo(*p*-phenylene vinylene) (OPV) chromophoric group to drive self-assembly *via* $\pi-\pi$ interactions, and a hydroxy functionality for interparticle hydrogen bonding. The OPV—Au particles reversibly self-assemble in *n*-heptane solution, forming shape persistent, spherical, nanometer-sized aggregates that do not collapse on a substrate. Optical absorption and transmission electron microscopy tomography studies show that the size and shape persistency can be tuned by modification of the ligands, adjustment of the core size, and variation of the concentration. The spherical assemblies can be manipulated with the tip of an atomic force microscope: an aggregate can be pushed over the surface for at least 20 times with nanometer precision and without substantial loss of material.

KEYWORDS: nanomanipulation · gold nanoparticles · self-assembly · π-conjugated oligomers · hybrid materials

Self-assembly is an appealing bottom-up approach to organize a variety of building blocks at the nanoscale.[1−3] Positioning self-assembled structures in a controlled fashion is, however, still a challenge. Nanomanipulation is an attractive tool to organize nanostructures and to address their properties. Scanning probe techniques including scanning tunneling microscopy (STM) and atomic force microscopy (AFM) can be used for such manipulation. Atoms and molecules can be positioned in a controlled fashion in a variety of nanostructures,[4] while inorganic nanoparticles can be pushed or swept[5−7] by an AFM tip. Chains and even words could be "written" on the nanoscale, and in some cases nanodevices were constructed by placing these structures between electrodes.[8] Combining self-assembly with nanomanipulation therefore seems an attractive approach for the construction of functional nanostructures with positional control.[9] However, assemblies of molecules or particles held together by noncovalent supramolecular interactions, are often too fragile to be manipulated by scanning probe microscopy.[10] The positioning of self-assembled objects has been achieved in solution using optical tweezers[11] and so-called probe manipulation.[12]

Hybrid nanoparticles based on inorganic and organic (semi)conductors have gained a lot of interest recently,[13] and the application into electronic devices is being explored intensively.[14−16] The self-assembly of such particles offers a tool to control the internal organization of these hybrid materials and thereby their macroscopic properties.[17−24] We have recently described that hybrid gold nanoparticles decorated with oligo(*p*-phenylene vinylene) (OPV) ligands, self-assemble into spherical aggregates in *n*-butanol[25] and water solution.[26] Transmission electron microscopy (TEM) showed that these soft assemblies collapse upon transfer from solution to the solid state. We have now synthesized gold nanoparticles functionalized with different OPVs in which the size of the inorganic gold core was varied as well (Chart 1). These OPV ligands containing hydroxy groups, are known to form stiff organogels in apolar solvents as a result of $\pi-\pi$-stacking, hydrogen bonding, and van der Waals interactions.[20,21] The resulting OPV—Au particles can be self-assembled reversibly in heptane solution yielding spherical, micrometer-sized aggregates with a tunable shape persistency. These unprecedented, shape-persistent, self-assembled objects were characterized by TEM tomography and, remarkably, could be moved

*Address correspondence to s.c.j.meskers@tue.nl, a.p.h.j.schenning@tue.nl.

Received for review June 28, 2010 and accepted October 13, 2010.

Published online October 22, 2010. 10.1021/nn101466s

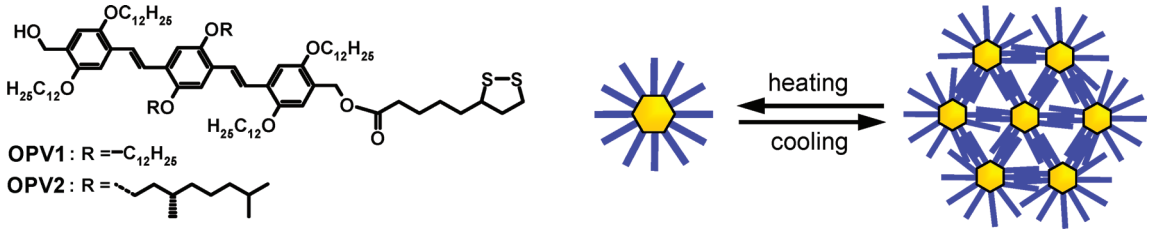

Chart 1. Chemical structure of two oligo(p-phenylene vinylene) (OPV) derivatives (OPV1 and OPV2), both bearing hydroxy and disulfide functionalities, with varying aliphatic side groups (left) and a cartoon illustrating the reversible self-assembly of the corresponding OPV−Au nanoparticles into shape persistent, spherical assemblies in heptane (right).

over the surface of the substrate by mechanical force applied *via* the tip of an AFM microscope.

RESULT AND DISCUSSION

Synthesis. The synthesis of **OPV1** (Chart 1) and the **OPV1−Au** particles with a gold core of 2.4 nm diameter have already been reported.[27] The synthesis of chiral **OPV2** is analogous to **OPV1**.[28,29] OPV−gold nanoparticle adducts (**OPV1−Au** and **OPV2−Au**) with different gold core sizes were obtained *via* two different methods.[30−34] In the first method, hydrogen tetrachloroaurate(III) was reduced by sodium borohydride in the presence of **OPV1** or **OPV2.**[18] In the second method first tetra-*n*-octylammonium bromide (TOAB)-capped gold nanoparticles were synthesized, and subsequently the TOAB was exchanged for **OPV1** or **OPV2**.[35] The size of the gold core of the **OPV1−Au** and **OPV2−Au** particles prepared by the first method was approximately 2.4 nm as determined by TEM. The second method yields metal cores characterized by an average diameter and standard deviation of 4.0 ± 0.9 nm (**OPV1−Au**) and 4.2 ± 1.1 nm (**OPV2−Au**).[22] The position of the surface plasmon (SP) absorption bands in toluene for the individual OPV−Au particles was consistent with the size estimated from TEM.[36] For the small particles a shoulder around $\lambda = 500$ nm is observed while a broad, more distinct peak centered at $\lambda = 526$ nm is obtained for the larger OPV−Au particles (Figure 1). Furthermore, in all cases the characteristic absorption band for trimeric OPVs could be discerned around 406 nm.[37]

Self-Assembly. UV−vis absorption spectroscopy showed that 2.4 nm **OPV1−Au** particles dispersed in *n*-heptane (2×10^{-5} M) were present as single species at elevated temperatures ($T \geq 40$ °C, Figure 2a). Under these conditions, the spectrum is similar to that obtained for dilute toluene solutions (Figure 1). Upon cooling, the gold surface plasmon band broadens and shifts to longer wavelengths, pointing to aggregation of the nanoparticles (Figure 2a).[12,38,39] This aggregation process was found to be reversible. At a lower concentration of the particles in solution (4 μM, Figure 2b), the broadening and redshift of the SP band is less pronounced. This indicates a smaller average size of the aggregates under these conditions. At a 1 μM concentration (Figure 2c), the changes in the SP band upon cooling are marginal. At these low concentrations, the spectra are virtually identical to those in toluene.

Self-assembled aggregates of the nanoparticles can be visualized by TEM on dried films of the **OPV1−Au** nanoparticles deposited from heptane solutions (2×10^{-5} M) on carbon-coated copper grids. TEM measurements at different tilt angle of the substrate (0°, 60°, and −60°, Figure 2) show that, in the dry state, the aggregates have a shape that is almost spherical with an average diameter of 1.02 ± 0.05 μm.[40] This remarkable feature indicates that the spherical nature of the aggregates expected to occur in solution is preserved after transfer to the amorphous carbon surface of the TEM grid. Apparently, here the introduction of a hydroxy functional group in the OPV ligands enforces the nanoparticle−nanoparticle interactions, making them

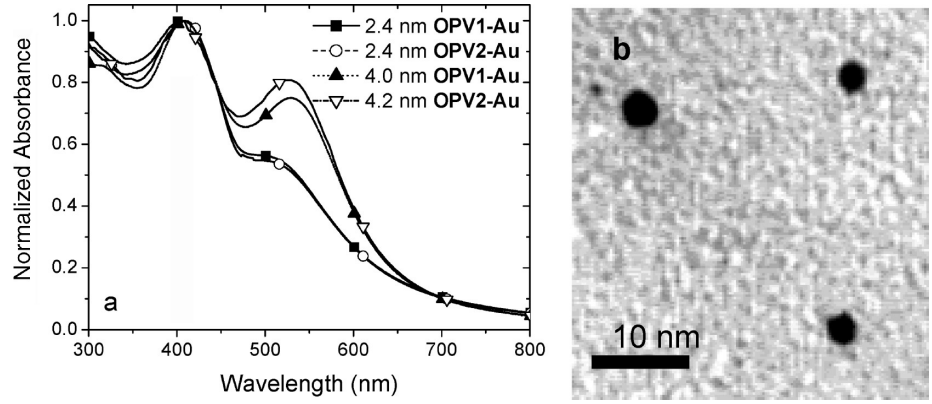

Figure 1. (a) Normalized UV−vis absorption spectra of OPV1−Au (d_{Au} = 2.4 and 4.0 nm) and OPV2−Au nanoparticles (d_{Au} = 2.4 and 4.2 nm) in toluene. (b) TEM image of the OPV−Au particles cast from dilute toluene solution with d_{Au} = 4 nm.

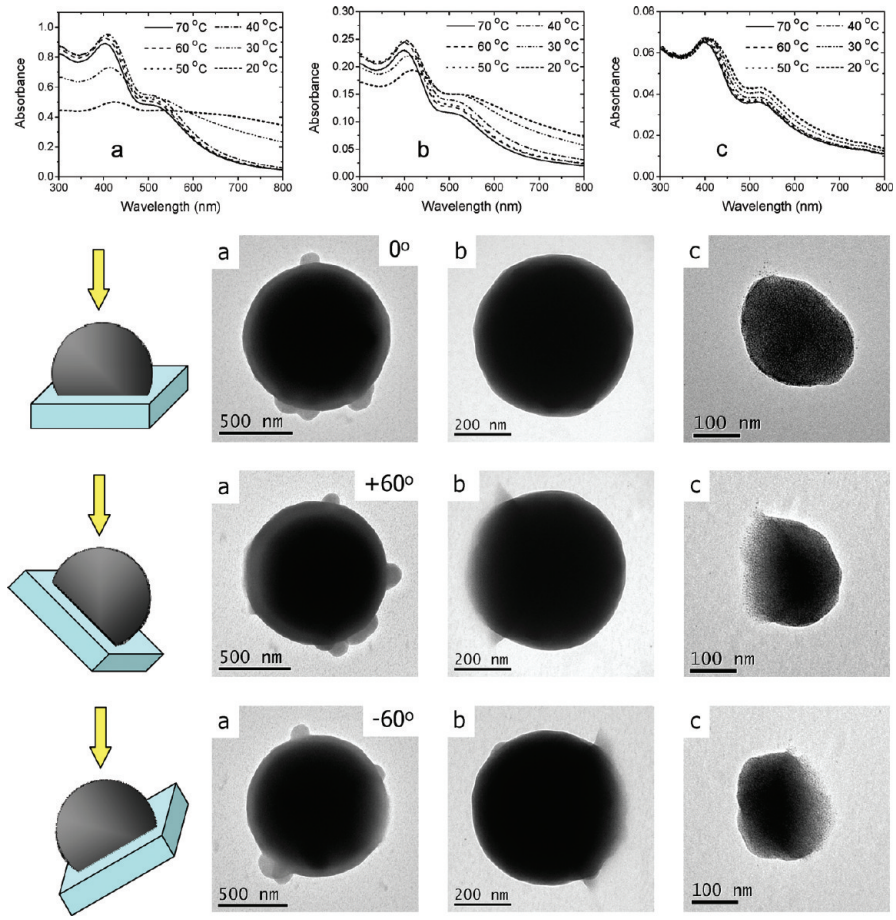

Figure 2. Self-assembly behavior of OPV1−Au nanoparticles with, d_{Au} = 2.4 nm at concentrations of 2 × 10^{-5} M (a), 4 μM (b), and 1 μM (c) in *n*-heptane. Top row: temperature dependent optical properties of the solutions (optical path length, 1 mm). Lower rows: corresponding TEM images at different tilt angles (0, 60, and −60°) on aggregates deposited from heptane solution.

stronger than the nanoparticle−substrate interactions. This results in a large "contact angle" and poor "wetting" as observed from the TEM tilt experiments. When depositing aggregates of **OPV1−Au** (d_{Au} = 2.4 nm) nanoparticles from heptane solutions with a lower concentration of nanoparticles, that is, 4 and 1 μM, TEM on the dry aggregates also shows spherical shapes with average diameters of 5.6 ± 0.9 × 10^2 and 2.4 ± 0.3 × 10^2 nm, respectively (Figures 2). This indicates that the diameter of the aggregates decreases upon lowering the concentration of the **OPV1−Au** particles. This trend corresponds with the inference made from the temperature dependent absorption studies (Figure 2). Curiously, TEM of the aggregates cast from dilute solution (1 μM, Figure 2c) indicates a diminished shape persistency.

Aggregates prepared from a 4 μM **OPV1−Au** solution in heptane were studied in more detail. The shape persistency of the spherical assemblies was confirmed by AFM imaging in tapping mode, on highly oriented pyrolytic graphite (HOPG), where heights of several hundreds of nanometers were measured (Figure 3a,b). In addition, dynamic light scattering (DLS) on the solutions used for deposition of the aggregates revealed that spherical objects with an average diameter of 5.4 ± 1.6 × 10^2 nm are present in solution (Figure 3c), in good agreement with the TEM results.[18,22] TEM imaging at higher magnifications, shows tight packing of the OPV−Au particles within the aggregates (Figure 3d). Incidentally, TEM at lower magnification shows that clustering of the micrometer-sized aggregates can occur (Figure 3e).

The data set on the **OPV1−Au** system allows us to analyze the self-assembly process in more detail. A plot of the average diameter and standard deviation of the aggregates as a function of the total concentration C_0 of **OPV1−Au** (Figure 3f) shows that the diameter increases with increasing C_0. A simple model for the association of monomeric units which features such behavior is the isodesmic (or equal *K*) model.[41] In this model—in the limit of high concentration—the average number of monomeric units in one aggregate varies as $\sqrt{C_0}$ in the limit of high C_0. This limit applies because the number of particles in the aggregates under study is large (>10^4). Then, for spherical aggregates, one expects the diameter of the aggregates to scale as $C_0^{1/6}$. This limiting behavior is illustrated in Figure 3e by the solid line. As can be seen, the trend predicted by

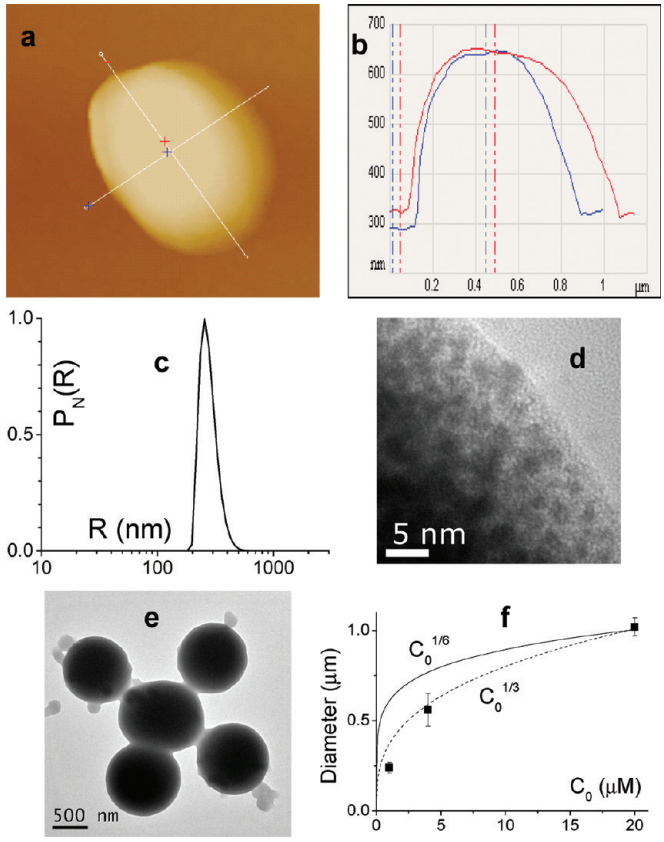

Figure 3. Atomic force micrograph of aggregates of OPV1−Au after deposition from heptane 4 μM, recorded in tapping mode (a), and the corresponding height cross sections in nm (b). Distribution function for the occurrence of aggregates of OPV1−Au as a function of radius *R* in *n*-heptane solution at 4 μM, as determined from dynamic light scattering (c). High magnification image taken at the edge of a spherical aggregate of OPV1−Au nanoparticles after deposition from *n*-heptane 4 μM (d). Clustering of aggregates deposited from a 2 × 10^{-5} M solution in *n*-heptane (e). Diameter of aggregates plotted *versus* the total concentration C_0 of OPV1−Au particles. Solid line, prediction from isodesmic model; dashed line, $d \propto C_0^{1/3}$ (f). For all graphs, d_{Au} = 2.4 nm.

the isodesmic model resembles the experimental data in a qualitative sense. Yet, upon closer inspection, the experimental data actually show a steeper dependence on C_0 than predicted by the model and apparently following a $C_0^{1/3}$ power law. In addition to this discrepancy, we also note that in the high concentration limit, the isodesmic model predicts a standard deviation for the diameter *d* that is equal to the mean value of *d*.[31,42] In contrast, the TEM and DLS data indicate a standard deviation in *d* smaller than 0.3*d*. We conclude that, although the isodesmic model is able to account qualitatively for the observed trend, it does not provide a complete description for the aggregation. A $C_0^{1/3}$ power law for the diameter of aggregates has also been observed for other systems[43] and can be interpreted in terms of long-range interactions.[44] In addition, aggregation can be influence by cooperativity[45] and by polydispersity in the size of the aggregating particles. For gold nanoparticles with a shell of organic ligands, their tendency to aggregate depends on the diameter of the particles.[46] Clearly, if this is the case, then for our polydisperse nanoparticles, the isodesmic model can only be an approximation. In this picture, aggregates will feature an outer shell of weakly bound, smaller nanoparticles that prevents further association of the cores containing mainly the larger particles.

By studying the aggregation behavior of **OPV1−Au** particles with a metal core of larger diameter we indeed find experimental evidence for the influence of the diameter of the gold core on the aggregation behavior. At a concentration of 0.5 μM, **OPV1−Au** particles with d_{Au} = 4.0 nm do form aggregates in *n*-heptane according to the absorption spectra (Figure 4a) while, at such low concentration, the **OPV1−Au** particles with d_{Au} = 2.4 nm do not yet self-assemble. At elevated temperatures ($T \geq 70$ °C), the 0.5 μM solution of 4.0 nm **OPV1−Au** in *n*-heptane showed a SP absorption band around λ = 524 nm, similar to what was observed in toluene (*vide supra*) and typical for particles of these dimensions. Below a temperature of 70 °C the SP band of the **OPV1−Au** particles broadened, indicating the formation of aggregates,[12,28] and at room temperature precipitation occurred readily. Furthermore, TEM imaging reveals aggregates with a diameter of 7.5 ± 0.8 × 10^2 nm for 4.0 nm **OPV1−Au** nanoparticles when cast from *n*-heptane solution with 0.5 μM concentration. In comparison, **OPV1−Au** with d_{Au} = 2.4 nm at the lowest concentration for which we have seen aggregate formation in TEM (1 μM), forms aggregates with 2.4 ± 0.3 × 10^2 nm diameter.

Influence of the Organic Ligand. An additional tool to influence the self-assembly behavior of the nanoparticles is to change the chemical structure of the organic ligands. Here we find that the introduction of branches in the side chains of the ligands (**OPV2**) reduces the shape persistency. UV−vis absorption experiments on **OPV2−Au** particles (d_{Au} = 2.4 ± 0.4 nm) show that, at a concentration of 2 × 10^{-5} M, the SP band is far less sensitive to changes in temperature (Figure 4b) when compared to the behavior of **OPV1−Au** particles (d_{Au} = 2.4 ± 0.6 nm, Figure 2a). This indicates that the driving force for aggregate formation is smaller for **OPV2−Au** in comparison with **OPV1−Au**. TEM on **OPV2−Au** also shows spherical aggregates, but with an average diameter that is somewhat smaller than for **OPV1−Au** (8.6 ± 1.1 × 10^2 nm *vs* 1.02 ± 0.05 μm, Figures 4b and 2a). Furthermore, TEM upon tilting the sample holder 60° and −60° shows a diminished "contact angle". We conclude that the branched side chains on the OPV, enhance the solubility and inhibit a tight packing of the aliphatic tails. This influence of the organic ligands can also be observed for **OPV2−Au** nanoparticles with a larger core (d_{Au} = 4.2 nm). When cast from a 0.5 μM *n*-heptane solution, we find evidence for aggregation of the 4.2 nm **OPV2−Au** particles into clusters with a diameter of 3.0 ± 0.6 × 10^2 nm (Figure 4c). In contrast, the 4.0 nm **OPV1−Au** nanoparticles form aggregates with 7.5 ± 0.8 × 10^2 nm diameter. This

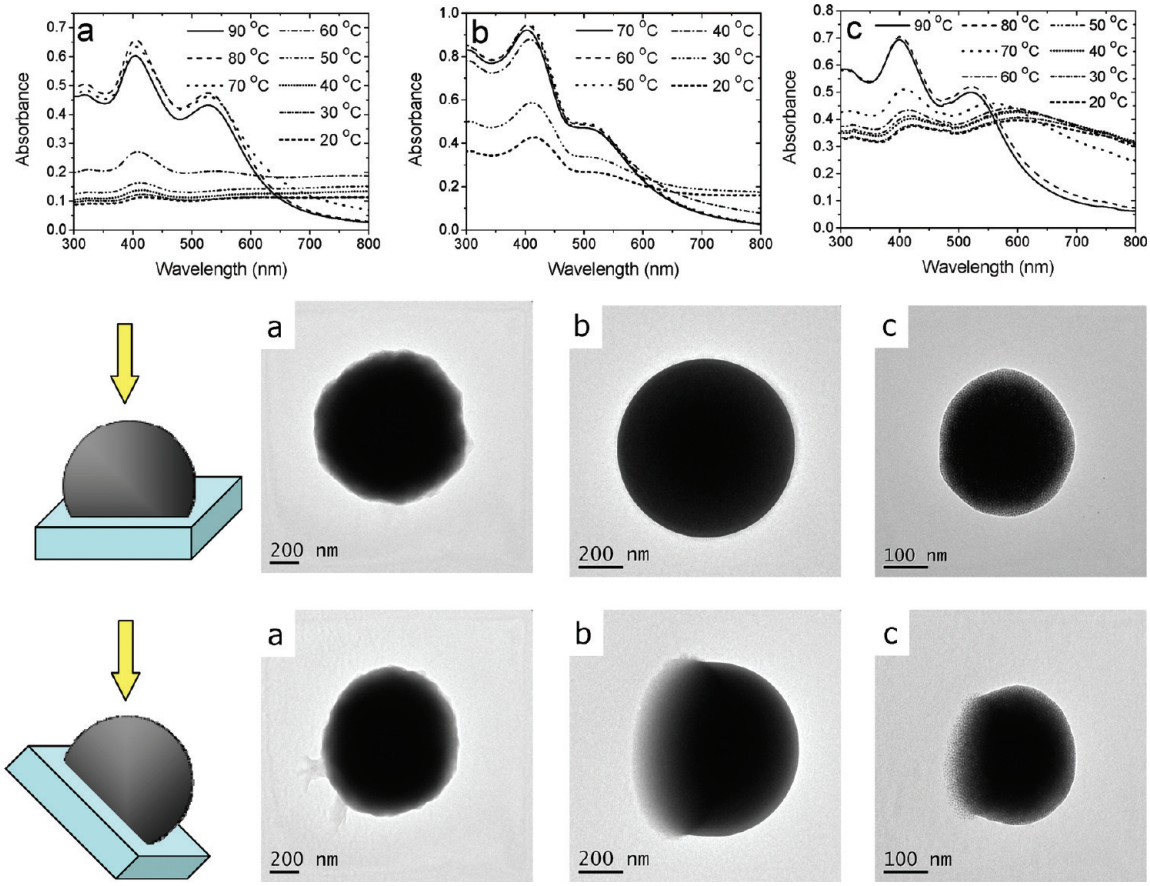

Figure 4. Self-assembly behavior of OPV1−Au nanoparticles, d_{Au} = 4.0 nm at concentrations of 0.5 μM (a), OPV2−Au nanoparticles, d_{Au} = 2.4 nm at concentrations of 2 × 10^{-5} M (b), and OPV2−Au nanoparticles, d_{Au} = 4.2 nm at concentrations of 0.5 μM (c). Top row: temperature dependent optical studies. Lower rows: corresponding TEM measurements at different tilt angles (0 and 60°), on aggregates deposited from *n*-heptane solution.

behavior is in accordance with earlier studies on the influence of side chains on gelation properties of OPVs,[21] indicating that the self-assembly can be tuned in a similar manner as for purely organic π-conjugated systems.[2]

The remarkable shape-persistent behavior was not observed for aggregates of OPV−Au particles without hydroxy functionality on the ligand and shorter branched side chains on the OPV moiety.[18,22] These latter aggregates collapse on apolar surfaces. Therefore, we conclude that the shape-persistent behavior is most likely the result of enforced interparticle interaction involving hydrogen bonding interactions. The simultaneous interactions between multiple hydroxyl groups will give rise to a so-called multivalent effect leading to an enhanced stability.[47] The interparticle interaction can be tuned by both the size of the inner metal core and also *via* the structure of the organic ligand. This suggests that the net interparticle force is the resultant of many types of interactions: van der Waals forces between the polarizable metal cores[36,48] and ligand−ligand interactions.[49−52] In our case, the ligand−ligand interactions comprise van der Waals effects, π−π stacking, and hydrogen bonding interactions. The latter seem to be of major importance for obtaining shape persistent aggregates.

Nanomanipulation by an AFM Tip. Since the **OPV1−Au** aggregates are remarkably stable and shape persistent, nanomanipulation experiments of these aggregates with the tip of an AFM microscope are carried out. For these experiments we have used two different types of surfaces.

The first type of substrate used is SiO_2 treated with octadecyltrichlorosilane in order to obtain a flat, apolar surface. **OPV1−Au** aggregates were deposited from a 2 × 10^{-5} M solution in *n*-heptane by drop-casting. Subsequent AFM measurements and manipulation confirmed the size and shape-persistency of the aggregates on this substrate. To this end, part of the surface was modified with triangular metal patterns deposited by photolithographic methods, before modifying the surface with octadecyltrichlorosilane. The pattern generated was such that the vertices of two triangles were at a spacing of 200 nm. As shown in Figure 5, this pattern facilitates the determination of the position of the aggregates upon manipulation. From a cluster of aggregates located about 7 μm from the gap between the metal triangles (Figure 5a), a particular aggregate was

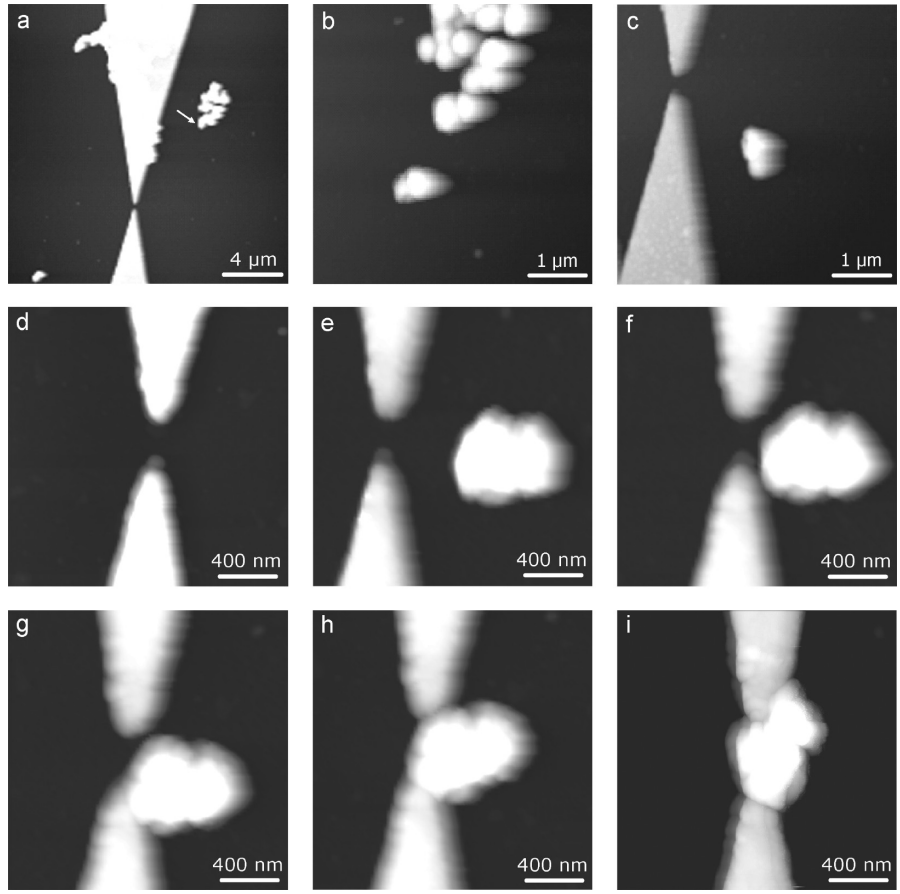

Figure 5. AFM images monitoring the different stages of the manipulation of an aggregate of 2.4 nm OPV1−Au nanoparticles with an AFM tip along an octadecyltrichlorosilane-coated SiO_2 surface after deposition from *n*-heptane (2×10^{-5} M). (a) Starting point. Arrow indicates the aggregate that has been pushed from the cluster of aggregates. (b,c) Intermediate stages of moving the aggregate toward a pair of photopatterned lithographic metal pads. (d) Zoom in on the pair of markers. (e−h) Intermediate stages of pushing the aggregate in between the metal markers on the Si substrate. (i) End point. The aggregate has been placed in between the pair of lithographic metal structures.

separated from the main group by the AFM tip next to the aggregate, operating in contact mode. This self-assembled hybrid aggregate could then be moved over the surface and pushed toward the spacing between the triangular metal patterns (Figure 5b,c). After pushing, the position of the particle was probed in tapping mode. Finally, by carefully taking small steps, the aggregate could be positioned between the pair of lithographic metal pads (Figure 5d−i).[22] The aggregate could be pushed at least 20 times without undergoing major changes and without losing parts.[53,54]

The second type of apolar surface that we have investigated is freshly cleaved HOPG. On this surface, **OPV1−Au** aggregates were deposited from a solution in *n*-heptane by drop-casting. Interestingly, using the AFM tip for manipulation, entire aggregates can be removed from this surface, leaving barely a trace indicating its original position. This is illustrated in Figure 6, where the white arrow illustrates the aggregate that is removed from the scan area by the tip. As can be seen only a very small amount of material is left behind on the surface after removal of the particle. From the experiment it did not become clear where the particle that was removed went. It could not be found in the 10×10 μm^2 scan area around the original position and might have been picked up with the AFM tip. Nevertheless, our results clearly illustrate the strength of the cohesion in the **OPV1−Au** aggregates yielding very stable hybrid nanospheres.

CONCLUSIONS

Gold nanoparticles functionalized with π-conjugated OPV segments have been self-assembled into spherical, shape persistent, nanometer-sized spherical aggregates in *n*-heptane. The shape persistent behavior is a result of simultaneous weak noncovalent interactions between the π-conjugated OPV segments giving rise to a multivalent effect leading to an enhanced stability. Interestingly, the shape persistency and size of these aggregates can be tuned by modification of either the organic ligands, the size of the metal core size, or by adjustment of the concentration. This illustrates the versatility of organic−inorganic nanohybrid materials. With the resulting properties it is possible to manipulate self-assembled aggregates with an AFM tip. Our method for creating shape-persistent ob-

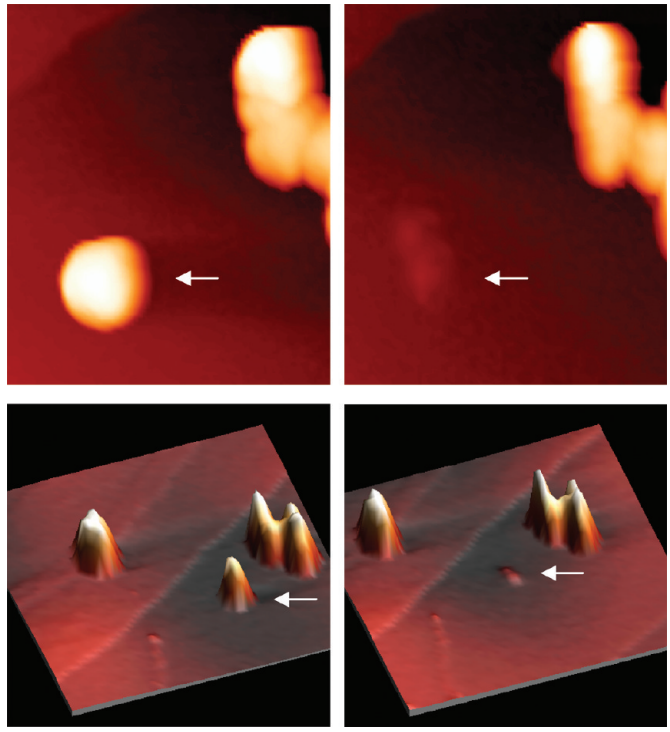

Figure 6. AFM manipulation of OPV1−Au aggregates (d_{Au} = 2.4 nm) on HOPG. Top row: 4 × 5 μm tapping mode images in top view; height scale, 0−300 nm. Bottom row: 10 × 10 μm² images in perspective. The left column shows the substrate before removal of the aggregate indicated by the white arrow, while the right column shows the sample after taking out this aggregate with the AFM tip in contact mode.

jects opens new possibilities for realizing nanosized plasmonics and/or electronics *via* combined self-assembly (bottom-up) and nanomanipulation (top-down) structuring.

Acknowledgment. This research has been supported by The Netherlands Organization for Scientific Research (NWO) through a grant in the Open Competition program. We acknowledge P. Bomans and N. Sommerdijk for the help with the TEM measurements and T. de Greef, R. Sijbesma, R. Janssen, and E. Meijer for stimulating discussions.

Supporting Information Available: Synthesis of **OPV2** and OPV−Au particles, experimental details on TEM, AFM nanomanipulation, DLS, and movie files showing the complete tilt TEM image series. This material is available free of charge *via* the Internet at http://pubs.acs.org.

REFERENCES AND NOTES

1. Whitesides, G. M.; Grzybowski, B. Self-Assembly at All Scales. *Science* **2002**, *295*, 2418–2421.
2. Hoeben, F. J. M.; Jonkheijm, P.; Meijer, E. W.; Schenning, A. P. H. J. About Supramolecular Assemblies of π-Conjugated Systems. *Chem. Rev.* **2005**, *105*, 1491–1546.
3. Schenning, A. P. H. J.; Meijer, E. W. Supramolecular Electronics; Nanowires from Self-Assembled π-Conjugated Systems. *Chem. Commun.* **2005**, 3245–3258.
4. Tseng, A. A.; Li, Z. J. Manipulations of Atoms and Molecules by Scanning Probe Microscopy. *Nanoscience Nanotech.* **2007**, *7*, 2582–2595.
5. Junno, T.; Carlsson, S.-B.; Xu, H.; Montelius, L.; Samuelson, L. Fabrication of Quantum Devices by Ångström-Level Manipulation of Nanoparticles with an Atomic Force Microscope. *Appl. Phys. Lett.* **1998**, *72*, 548–550.
6. Mougin, K.; Gnecco, E.; Rao, A.; Cuberes, M. T.; Jayaraman, S.; McFarland, E. W.; Haidara, H.; Meyer, E. Manipulation of Gold Nanoparticles: Influence of Surface Chemistry, Temperature, and Environment (Vacuum *versus* Ambient Atmosphere). *Langmuir* **2008**, *24*, 1577–1581.
7. Rubio-Sierra, F. J.; Heckl, W. M.; Stark, R. W. Nanomanipulation by Atomic Force Microscopy. *Adv. Eng. Mater.* **2005**, *7*, 193–196.
8. Zabet-Khosousi, A.; Dhirani, A. Charge Transport in Nanoparticle Assemblies. *Chem. Rev.* **2008**, *108*, 4072–4124.
9. Heckl, W. M. Molecular Self-Assembly and Nanomanipulation—Two Key Technologies in Nanoscience and Templating. *Adv. Eng. Mater.* **2004**, *6*, 843–847.
10. For example: Lamnotagne, C.-A.; Cuerrier, C. M.; Grandbois, M. AFM as a Tool To Probe and Manipulate Cellular Processes. *Pflug. Arch.—Eur. J. Physiol.* **2008**, *456*, 61–70.
11. For example: Schenning, A.P.H. J.; Jonkheijm, P.; Hofkens, J.; De Feyter, S.; Asavei, T.; Cotlet, M.; De Schryver, F. C.; Meijer, E. W. Formation and Manipulation of Supramolecular Structures of Oligo(*p*-phenylenevinylene) Terminated Poly(propylene imine) Dendrimers. *Chem. Commun.* **2002**, 1264–1265.
12. Reynolds, K.; Komulainen, J.; Lovera, P.; Iacopino, D.; Pudas, M.; Vahakangas, J.; Redmond, G. Probe Based Manipulation and Assembly of Nanowires into Organized Mesostructures. *Nanotechnology* **2008**, *19*, 485301 (10pp).
13. For a review see: Sih, B. C.; Wolf, M. O. Metal Nanoparticle-Conjugated Polymer Nanocomposites. *Chem. Commun.* **2005**, 3375–3384.
14. For an example on solar cells: Huynh, W. U.; Dittmer, J. J.; Alivisatos, A. P. Hybrid Nanorod-Polymer Solar Cells. *Science* **2002**, *295*, 2425–2427.
15. For an example on light emitting diodes: Dabbousi, B. O.; Bawendi, M. G.; Onitsuka, O.; Rubner, M. F. Electroluminescence from CdSe Quantumdot/Polymer Composites. *Appl. Phys. Lett.* **1995**, *66*, 1316–1318.
16. For an example of electronic memories: (A) Tseng, R. J.; Huang, J.; Ouyang, J.; Kaner, R. B.; Yang, Y. Polyaniline Nanofiber/Gold Nanoparticle Nonvolatile Memory. *Nano Lett.* **2005**, *5*, 1077–1080.

17. Westerlund, F.; Bjornholm, T. Directed Assembly of Gold Nanoparticles. *Curr. Opin. Coll. Interface Sci.* **2009**, *14*, 126–134.
18. Schmid, G.; Simon, U. Gold Nanoparticles: Assembly and Electrical Properties in 1−3 Dimensions. *Chem. Commun.* **2005**, 697–710.
19. Kotov, N. A.; Stellacci, F. Frontiers in Nanoparticle Research: Toward Greater Complexity of Structure and Function of Nanomaterials. *Adv. Mater.* **2008**, *20*, 4221–4222.
20. For a review see: Descalzo, A. B.; Martínez-Máñez, R.; Sancenón, F.; Hoffmann, K.; Rurack, K. The Supramolecular Chemistry of Organic-Inorganic Hybrid Materials. *Angew. Chem., Int. Ed.* **2006**, *45*, 5924–5948.
21. Barth, J. V.; Costantini, G.; Kern, K. Engineering Atomic and Molecular Nanostructures at Surfaces. *Nature* **2005**, *437*, 671–679.
22. Sone, E. D.; Zubarev, E. R.; Stupp, S. I. Semiconductor Nanohelices Templated by Supramolecular Ribbons. *Angew. Chem., Int. Ed.* **2002**, *41*, 1705–1709.
23. Duan, X.; Huang, Y.; Cui, Y.; Wang, J.; Lieber, C. M. Indium Phosphide Nanowires as Building Blocks for Nanoscale Electronic and Optoelectronic Devices. *Nature* **2001**, *409*, 66–69.
24. Huang, Y.; Duan, X.; Cui, Y.; Lauhon, L. J.; Kim, K.-H.; Lieber, C. M. Logic Gates and Computation from Assembled Nanowire Building Blocks. *Science* **2001**, *294*, 1313–1317.
25. van Herrikhuyzen, J.; Janssen, R. A. J.; Meijer, E. W.; Meskers, S. C. J.; Schenning, A. P. H. J. Fractal-like Self-Assembly of Oligo(*p*-phenylene vinylene)-Capped Gold Nanoparticles. *J. Am. Chem. Soc.* **2006**, *128*, 686–687.
26. Jakobs, R. T. M.; van Herrikhuyzen, J.; Gielen, J. C.; Christianen, P. C. M.; Meskers, S. C. J.; Schenning, A. P. H. J. Self-Assembly of Amphiphilic Gold Nanoparticles Decorated with a Mixed Shell of Oligo(*p*-phenylenevinylene)s and Ethyleneoxide Ligands. *J. Mater. Chem.* **2008**, *18*, 3438–3441.
27. van Herrikhuyzen, J.; George, S. J.; Vos, M. R. J.; Sommerdijk, N. A. J. M.; Ajayaghosh, A.; Meskers, S. C. J.; Schenning, A. P. H. J. Self-Assembled Hybrid Oligo(*p*-phenylenevinylene)−Gold Nanoparticle Tapes. *Angew. Chem., Int. Ed.* **2007**, *46*, 1825–1828.
28. George, S. J.; Ajayaghosh, A.; Jonkheijm, P.; Schenning, A. P. H. J.; Meijer, E. W. Coiled-Coil Gel Nanostructures of Oligo(*p*-phenylenevinylene)s: Gelation Induced Helix Transition in a Higher-Order Supramolecular Self-Assembly of a Rigid π-Conjugated System. *Angew. Chem., Int. Ed.* **2004**, *43*, 3422–3425.
29. See supporting information.
30. Brust, M.; Walker, M.; Bethell, D.; Schiffrin, D. J.; Whyman, R. J. Synthesis of Thiol Derivatized Gold Nanoparticles in a Two-Phase Liquid/Liquid System. *J. Chem. Soc., Chem. Commun.* **1994**, 801–802.
31. Hostetler, M. J.; Wingate, J. E.; Zhong, C.-J.; Harris, J. E.; Vachet, R. W.; Clark, M. R.; Londono, J. D.; Green, S. J.; Stokes, J. J.; Wignall, G. D.; *et al.* Alkanethiolate Gold Cluster Molecules with Core Diameters from 1.5 to 5.2 nm: Core and Monolayer Properties as a Function of Core Size. *Langmuir* **1998**, *14*, 17–30.
32. Fink, J.; Kiely, C. J.; Bethell, D.; Schiffrin, D. J. Self-organization of Nanosized Gold Particles. *Chem. Mater.* **1998**, *10*, 922–926.
33. Thomas, K. G.; Kamat, P. V. Making Gold Nanoparticles Glow: Enhanced Emission from a Surface-Bound Fluoroprobe. *J. Am. Chem. Soc.* **2000**, *122*, 2655–2656.
34. Montalti, M.; Prodi, L.; Zaccheroni, N.; Battistini, G. Modulation of the Photophysical Properties of Gold Nanoparticles by Accurate Control of the Surface Coverage. *Langmuir* **2004**, *20*, 7884–7886.
35. van Herrikhuyzen, J.; Janssen, R. A. J.; Schenning, A. P. H. J.; Meskers, S. C. J. Picosecond Energy Transfer in Oligo(*p*-phenylenevinylene) Capped Gold Nanoparticles. *Chem. Phys. Lett.* **2007**, *433*, 340–344.
36. Link, S.; El-Sayed, M. A. Size and Temperature Dependence of the Plasmon Absorption of Colloidal Gold Nanoparticles. *J. Phys. Chem. B.* **1999**, *103*, 4212–4127.
37. Schenning, A. P. H. J.; Jonkheijm, P.; Peeters, E.; Meijer, E. W. Hierarchical Order in Supramolecular Assemblies of Hydrogen-Bonded Oligo(*p*-phenylene vinylene)s. *J. Am. Chem. Soc.* **2001**, *123*, 409–416.
38. Shipway, A. N.; Lahav, M.; Gabai, R.; Willner, I. Investigations into the Electrostatically Induced Aggregation of Au Nanoparticles. *Langmuir* **2000**, *16*, 8789–8795.
39. Park, S. Y.; Lee, J. S.; Georganopoulou, D.; Mirkin, C. A.; Schatz, G. C. Structures of DNA-Linked Nanoparticle Aggregates. *J. Phys. Chem. B* **2006**, *110*, 12673–12681.
40. A movie of the complete tilt series of 4 μM **OPV1−Au** (d_{Au} = 2.4 nm) can be found in the Supporting Information.
41. Ciferri, A. *Supamolecular Polymers*, 2nd ed.; CRC Press: Boca Raton, FL, 2005; Chapter 2.
42. Sheu, W.-S. Molecular Weight Averages and Polydispersity of Polymers. *J. Chem. Educ.* **2001**, *78*, 554–555.
43. Stradner, A.; Sedgwick, H.; Cardinaux, F.; Poon, W. C. K.; Egelhaaf, S. U.; Schurtenberger, P. Equilibrium Cluster Formation in Concentrated Protein Solutions and Colloids. *Nature* **2004**, *432*, 492–495.
44. Rahedi, A. J.; Douglas, J. F.; Starr, F. W. Model for Reversible Nanoparticle Assembly in a Polymer Matrix. *J. Chem. Phys.* **2008**, *128*, 024902.
45. Douglas, J. F.; Dudowicz, J.; Freed, K. F. Lattice Model of Equilibrium Polymerization. VII. Understanding the Role of "Cooperativity" in Self-Assembly. *J. Chem. Phys.* **2008**, *128*, 224901–224917.
46. Ohara, P. C.; Leff, D. V.; Heath, J. R.; Gelbart, W. M. Crystallization of Opals from Polydisperse Nanoparticles. *Phys. Rev. Lett.* **1995**, *75*, 3466–3469.
47. Mulder, A.; Huskens, J.; Reinhoudt, D. N. Multivalency in Supramolecular Chemistry and Nanofabrication. *Org. Biomol. Chem.* **2004**, *2*, 3409–3424.
48. Kim, H.-Y.; Sofo, J.; O. Velegol, D.; Cole, M. W.; Lucas, A. A. Van der Waals Dispersion Forces between Dielectric Nanoclusters. *Langmuir* **2007**, *23*, 1735–1740.
49. Luedtke, W. D.; Landman, U. Structure, Dynamics, and Thermodynamics of Passivated Gold Nanocrystallites and their Assemblies. *J. Phys. Chem.* **1996**, *100*, 13323–13329.
50. Schapotschnikow, P.; Pool, R.; Vlugt, T. J. H. Molecular Simulations of Interacting Nanocrystals. *Nano Lett.* **2008**, *8*, 2930–2934.
51. Landman, U.; Luedtke, W. D. Small Is Different: Energetic, Structural, Thermal, and Mechanical Properties of Passivated Nanocluster Assemblies. *Faraday Discuss.* **2004**, *125*, 1–9.
52. Mueggenburg, K. E.; Lin, X.-M.; Goldsmith, R. H.; Jaeger, H. M. Nanocrystal Superlattices: Assembly at Liquid Interfaces. *Nat. Mater.* **2007**, *6*, 656–660.
53. For a 3D image, see Supporting Information.
54. Preliminary electrical conductivity measurements of nanoparticle assemblies between the metal electrodes gave inconclusive results.